

Experimental Study of Co-Flow Jet Airfoil Performance Enhancement Using Discrete Jets

Bertrand P. E. Dano¹, Gecheng Zha² and Michael Castillo³
University of Miami, Coral Gables, FL 33124, USA
gzha@miami.edu
www7.miami.edu/ftp/acfdlab

Abstract: This paper demonstrates a new performance enhancement methodology for Co-Flow Jet (CFJ) airfoils using discrete injection jets. This research is motivated by the hypothesis that a discrete CFJ (DCFJ) airfoil will generate both streamwise and spanwise vortex structures to achieve more effective turbulent mixing than an open slot CFJ airfoil. Aerodynamic forces and DPIV measurements show that the DCFJ airfoil can achieve up to a 250% increase of maximum lift, and simultaneously generates a tremendous thrust. Nearly 80% of the injection momentum is converted to drag reduction, which indicates that CFJ airfoils are highly energy efficient. The stall angle of attack is also significantly increased. In other words, a DCFJ airfoil is a high lift system and at the same time is also a high thrust propulsion system with low energy expenditure. Best performances are achieved with small discrete holes and large obstruction factor. Power consumption is analyzed and is found to be low compared with the performance gain. Thus, the DCFJ airfoil concept appears to be very promising for the development of integrated airframe-propulsion systems and rotorcraft systems with high performance and high efficiency.

Nomenclature

AoA	Angle of attack
C	Chord length
CFJ	Co-flow jet
CC	Circulation control
C_L	Lift coefficient
C_D	Drag coefficient
C_μ	Jet momentum coefficient
C_μ^*	Jet momentum coefficient for open slot CFJ

¹ Adjunct Faculty, Dept. of Mechanical and Aerospace Engineering

² Associate Professor, Dept. of Mechanical and Aerospace Engineering

³ Undergraduate Student, Dept. of Mechanical and Aerospace Engineering

D	Drag
L	Lift
M	Mach number
p	Static pressure
P	Power consumption
P_c	Power coefficient
P_t	Total pressure
Re	Reynolds number
S	Wing span area
\dot{m}	Jet mass flow rate
u, v, w	Velocity components in x-, y-, and z-direction
V_{jet}	Velocity vector
V_{jet}^*	Velocity vector for open slot CFJ
x, y, z	chord, normal and spanwise directions, with respect to the airfoil
η	Drag reduction efficiency
η_p	Pump efficiency
Subscripts	
∞	Freestream

I. Introduction

Over the past decade, a large number of flow control techniques for airfoil performance enhancement have shown breakthroughs from conventional aerodynamic constraints and achieves drastic performance enhancement [1, 2, 3, 4, 5, 6, 7]. Various flow control techniques have been pursued recently including zero-net mass flux (ZNMF) synthetic jets [8] using acoustic wave excitation and dielectric-barrier discharge plasma actuators [9, 10]. In recent years, pulsed fluidic actuators are beginning to deliver effective mixing and performance enhancement for realistic high Reynolds number flows [11, 12]. Circulation control (CC) [13-16] airfoils driven by fluidic actuators have been studied for more than three decades with the goal of increasing airfoil lift [15, 16,]. However, a CC airfoil still needs trailing edge flaps to create the curvature for the Coanda effect.

The key idea behind all flow control technology (passive or active) is to achieve increased lift, increased stall margin, and reduced drag with low energy expenditure and minimal solid structure device. The latter one imposes weight penalty, system complication, and parasite drag when not in use. Furthermore, the energy consumption of the different flow control methods is rarely addressed.

Co-Flow Jet (CFJ) Airfoil

Among all these new techniques, the co-flow jet technology, developed by Zha et al. has shown promising results [17-23]. Based of fluidic actuators generating simultaneous blowing at the leading edge (LE) and suction near the trailing edge (TE), zero net mass flux (ZNMF) is achieved over the extrado of the airfoil. A schematic of a

CFJ airfoil concept is shown in Fig. 1. The jet injection behind LE suction peak and jet suction near TE provides a unique mechanism to minimize the jet pumping energy expenditure, because the jet injection is at the lowest pressure location and jet suction is at the highest pressure location of an airfoil. The implementation of CFJ technology on an actual airplane can be obtained by using highly pressurized air from the engines for the jet injection, while the air intake of the turbine creates the suction. Alternatively, a pump can be imbedded in the wing structure, and circulate the air. For either technique, the power required for activation and the net loss from propulsion needs to be addressed.

Performance enhancement was shown to reach several times maximum lift increase and a tremendous thrust generated at low angle of attack (AoA). These results suggest that the CFJ airfoil is not only an excellent lift enhancement device, but also a very effective thrust generator.

The fundamental mechanism of CFJ airfoil is that the severe adverse pressure gradient on the suction surface augments turbulent shear layer mixing and diffusion between the main flow and the jet. The mixing creates a lateral transport of energy from the jet to the main flow and allows the main flow to overcome the large adverse pressure gradient and remain attached even at very high AoA. Hence, the stall margin is significantly increased. At the same time, the high momentum jet drastically increases the circulation, which significantly augments lift, reduces drag or even generates thrust (net negative drag) due to the filled wake and the supersuction at airfoil LE. The portion of CFJ energy used to overcome the increased drag due to higher jet speed is very small since the mixing occurs immediately when the jet penetrates into the boundary layer under the adverse pressure gradient. With higher mixing more energy is transferred from the jet to the main flow, resulting in lower energy loss to drag.

The CFJ airfoil has already proved to be a valuable solution for the development of high efficiency, low emission and low noise aircraft. Several futuristic high performance aircraft concepts using integrated airframe propulsion system based on CFJ airfoil are given in [24-27]. So far, all the experimental and numerical research on CFJ airfoils has used open slot injection. That is the injection slot is a single opening along the entire airfoil span. Since the CFJ airfoil flow control is still in an early stage of development, it is expected that significant performance enhancement can be obtained once this technology has matured.

Discrete CFJ (DCFJ) Airfoil

Discretization of the open-slot CFJ was accomplished by inserting tabs of different sizes in the open slot to achieve various injection jet sizes. A close-up photo of discrete injection holes with tabs in place is shown in Fig. 2. As previously mentioned, the turbulent mixing between the jet and the main flow is the fundamental mechanism for CFJ airfoil performance enhancement. The open slot uniform CFJ airfoil may have a 2-dimensional jet mixing along span with coherent vortex structure due to dissimilarity of two jet parameters (e.g., density, velocity, etc) [28]. A coherent vortex generates predominantly spanwise vorticity even though the large vortex structure is 3-dimensional. A discrete jet penetrating into the main flow can also generate streamwise large vortices [29]. Fig. 4 shows the flow visualization of wind tunnel test by Dano et al. [29], which shows that two counter-rotating vortices are induced by an inclined pulsed jet in cross flow (JICF).

As sketched in Fig. 5, the hypothesis of a discrete jet is that it will generate both strong streamwise and spanwise vorticity, which will produce stronger flow entrainment and flow mixing. Hence, it is expected that a discrete CFJ (DCFJ) will be a more effective means to transfer energy from the jet to the main flow, which will result in more lift enhancement and drag reduction at lower energy expenditure.

The purpose of this research is to demonstrate the increased performance enhancement and reduced energy expenditure resulted from using discrete jets instead of open slot uniform CFJ for airfoil flow control. Aerodynamic performance is examined for different configurations, and the corresponding power requirements are evaluated.

II. Experiment Setup and Analysis

Wind tunnel and airfoil setup

Pressurized air is injected in a spanwise long cavity near the LE, and then exits through a spanwise long rectangular slot. A Duocel high density aluminum foam (HDF) was placed between the inlet and the injection slot to equilibrate the pressure and ensure a uniform exit velocity. Similarly, a spanwise long cavity placed near the TE is used to let the air settle down before being sucked through three suction ports. The airfoil used for baseline comparison was a NACA 6415 with the chord length of 0.3048 m and span of 0.5906 m. The CFJ airfoil was a NACA 6415 with CFJ implementation located at 7.5% and 88.5% of the chord for injection and suction, respectively. The injection and suction slot heights were 0.65% (2.0 mm) and 1.42% (4.0 mm) of the chord, respectively.

All airflow and aerodynamic variables were acquired at the University of Miami 24"x24" wind tunnel facilities. The injection and suction flow conditions were independently controlled. A compressor supplies the injection flow line and the flow rate controlled using a Koso™ Hammel Dahl computer controlled valve. A vacuum pump generates the necessary low pressure for suction and is controlled with a manual needle valve. Both mass flow rates in the injection and suction lines are measured using Oripac™ orifice mass flowmeters equipped with high precision MKS pressure transducers. Total pressure and temperature probes were placed inside the injection and suction cavities as shown in Fig. 3. The aerodynamics variables are measured using an AMTI™ 6 component transducer. All wind tunnel freestream, CFJ airflow and aerodynamic variables were recorded using a state-of-the-art Labview™ data acquisition system. All the data (e.g., wind tunnel speed, aerodynamic forces, blowing and suction mass flow rates) were acquired at a rate of approximately 50 samples per seconds, allowing for limited airfoil flutters analysis around stall angle(s).

Various laser flow visualization techniques were used to monitor the flow field over the suction surface. A LaVision Digital Particle Image Velocimetry (DPIV) system with a Litron Nano Nd:YAG 200 mJ/pulse was used to monitor and acquire the velocity field surrounding the airfoil. An adaptive 32x32 to 16x16 pixels cross-correlation analysis method was used with masking of the airfoil, resulting in a 150x200 vectors (including the airfoil). A 1,000 instantaneous velocity fields were acquired for each AoA and each jet momentum coefficient.

Open slot CFJ and DCFJ parameters

The range of angle of attack (AoA) was varied between 0° to 35°. Nominal free stream velocity was $V_\infty = 10$ m/s for all tests and the chord Reynolds number was about 195,000. Even though this Reynolds number is in the transitional range, the LE trip was not implemented after we had observed that the measured difference with and without trip is negligible for the flow control tests.

The jet momentum coefficient C_μ was defined as:

$$C_\mu = \frac{\dot{m} V_{\text{jet}}}{\frac{1}{2} \rho_\infty V_\infty^2 S} \quad (1)$$

where \dot{m} is the jet mass flow rate, V_{jet} is the jet velocity, ρ_∞ is the free stream density, V_∞ is the free stream velocity, and S is the planform area of the airfoil. The obstruction factors (OF) is defined as the blocked area divided by the original CFJ open slot area. For a given mass flow rate, increasing OF will result in an increase in jet exit velocity due to decreased jet exit area. Therefore, C_μ will change when OF is changed even if \dot{m} is kept constant. For comparison purposes, the jet momentum coefficient for the open slot CFJ will be used and defined as:

$$C_\mu^* = \frac{\dot{m} V_{\text{jet}}^*}{\frac{1}{2} \rho_\infty V_\infty^2 S} \quad (2)$$

where the superscript * stand for open slot CFJ airfoil. For a given OF, a large number of configurations can be obtained depending on the number of jet injection holes and the hole sizes. Table 1 shows the list of the OF presented here, ranging from 1/5 to 3/4, and the hole sizes. For each OF, we tested two configurations containing the larger (hereafter labeled A) and smaller number of discrete jets (hereafter labeled B). Mass flow rates of $\dot{m} = 0$ kg/s, 0.030 kg/s, 0.045 kg/s and 0.060 kg/s are used. Corresponding open slot CFJ airfoil momentum coefficients are $C_\mu^* = 0, 0.08, 0.16$ and 0.30 , respectively. Table 2 shows the values of C_μ and C_μ^* and the corresponding jet exit velocity for all discrete CFJ configurations. In order to characterize even more the performance enhancement of the CFJ and DCFJ compared to baseline, the following drag reduction efficiency parameter are defined:

$$\eta = \frac{C_{D\text{baseline}} - C_{D\text{DCFJ}}}{C_\mu} \quad (3)$$

This quantity describes the efficiency of drag reduction at the energy cost to pump the jet with the momentum coefficient of C_μ . In other words, it is a measure of how much injection jet momentum is absorbed as the drag reduction. Note that the denominator is the actual C_μ , not C_μ^* .

Table 1. Matrix of discrete CFJ configuration

Name	OF	Config	# of jets	Hole width mm (% cord)	Schematic representation (openings are injection holes, solid lines are tabs)
DCFJ 1/5	1/5	A	5	94.5 (16.0%)	
		B	2	236.2 (40.0%)	
DCFJ 1/3	1/3	A	10	43.7 (7.4%)	
		B	5	98.4 (16.7%)	
DCFJ 1/2	1/2	A	19	15.5 (2.6%)	
		B	3	98.4 (16.7%)	
DCFJ 2/3	2/3	A	19	10.4 (1.76%)	
		B	9	21.9 (3.7%)	
DCFJ 3/4	3/4	A	14	10.5 (1.79%)	
		B	5	29.5 (5.0%)	

Table 2. Corresponding C_μ and C_μ^* for discrete CFJ configurations

\dot{m} (kg/s)	C_μ^* and V_{jet} (Open Slot)	C_μ and V_{jet} (Discrete CFJ)				
		DCFJ 1/5	DCFJ 1/3	DCFJ 1/2	DCFJ 2/3	DCFJ 3/4
0.030	0.08 (25m/s)	0.11 (29m/s)	0.13 (38m/s)	0.17 (52m/s)	0.23 (73m/s)	0.34 (106m/s))
0.045	0.16 (33m/s)	0.21 (43m/s)	0.23 (51m/s)	0.30 (69m/s)	0.49 (109m/s)	0.67 (153m/s)
0.060	0.30 (46m/s)	0.36 (56m/s)	0.41 (69m/s)	0.58 (97m/s)	0.89 (150m/s)	1.32 (231m/s)

Power consumption

The power consumption of the pump to drive the CFJ jet can be defined as:

$$P = \frac{\dot{m} C_p T_1}{\eta_p} \left(\Gamma^{\frac{\gamma-1}{\gamma}} - 1 \right) \quad (4)$$

where C_p is the specific heat capacity at constant pressure, taken to be 1003.4 J/kg/K, γ is the ratio of specific heats valued at 1.4, and η_p is the pump efficiency, $\Gamma = \frac{p_{01}}{p_{02}}$ is the ratio of the total pressures p_{01} and p_{02} corresponding to the jet injection and suction, respectively. The total pressures were measured inside the injection/suction cavities (locations 1 and 2 in Fig. 3). The total temperature T_1 was measured using a

thermocouple in the vicinity of the pressure probe location. Similar to the lift and drag coefficient, a power coefficient is defined as:

$$P_c = \frac{P}{\frac{1}{2} \rho_\infty V_\infty^3 S} \quad (5)$$

III. Results

Flow visualizations and DPIV results

A few examples of flow visualization and DPIV are presented here to illustrate the mechanism responsible for the performance increase. Fig. 6 and 7 shows the difference in flow structure along a discrete jet and over a tab, respectively. The jet flow was not seeded resulting in increased contrast for flow visualization, however this slightly degraded the DPIV velocity results in the vicinity of the jet exit. One can see that the flow within the jet plan is dominated by coherent vortices that develop along the airfoil surface and break down further downstream, effectively increasing the turbulent mixing of the wall jets. The flow over a tab blocking the open slot also appears to be dominated by turbulent vortices, comprising both streamwise and spanwise (coherent) vortices. While the spanwise vortices are clearly shown, the streamwise vortices lay in a plan perpendicular to the images and can not be easily shown.

Simultaneous flow visualization, PIV velocity field, CL and CD were acquired during a DCFJ activation sequence. Fig. 8 shows two examples of the combined results for DCFJ 2/3 with $C_{\mu}^* = 0.16$ and $AoA = 25^\circ$. Fig. 8a shows the state of the flow prior to activation, and exposes a largely separated flow with a low lift and high drag. Fig. 8b shows the results after the DCFJ was activated. One can see that the flow is attached and the velocity along the surface is in excess of 2-3 times the main stream velocity. Notice that the jet injection activation is practically instantaneous, but full suction is not obtained until approximately 15s. This is due to the large vacuum tank used between the pump and the airfoil. Nonetheless, a 250% increase in lift is observed while drag decreases to negligible values. Note that, at lower AoA, the measured drag is decreased to negative values.

Aerodynamic Performance

Jet Size Effect

The jet size effect on the performance was investigated and the results are shown in Fig. 9. For most cases, the configurations with higher number of discrete jets (A) systematically generate more lift than the alternate configurations (B). This is because configuration A with smaller jet size generates higher jet velocity, higher entrainment, stronger jet mixing, and thus higher circulation. This trend increases as the value of C_{μ}^* is increased. Overall, a lift increase between 10% and 40% over the open slot CFJ airfoil can be obtained using configuration A instead of B. For increased OF, the difference between the two configurations seems to decrease with increasing AoA. These results

suggest that smaller size jets with higher jet velocity are more effective to enhance lift. Consequently, only configuration A is analyzed in the subsequent sections.

Obstruction Factor (OF) Effect on Lift

Lift coefficient C_L for baseline, open slot and all DCFJ configurations are grouped together in Fig. 10. Compared to open slot CFJ, DCFJ 1/5 and DCFJ 1/3 show a small decrease in lift for all C_{μ}^* and all AoA except past the stall angle ($AoA \approx 25^\circ$). For DCFJ 1/2, a clear increase in lift can be observed for all AoA. This trend increases for increasing values of C_{μ}^* . Finally, DCFJ 2/3 and DCFJ 3/4 show a substantial lift increase over the open slot CFJ for all AoA and all C_{μ}^* .

Evaluation of the lift performance increase for DCFJs compared to baseline and open slot CFJ are shown in Fig. 11. From Fig. 11 it is evident that the CFJ airfoil is very effective to increase lift, in particular the DCFJ airfoil.

Increasing C_{μ}^* and OF systematically provides an increase in lift. Notice that, the difference between DCFJ 2/3 and DCFJ 3/4 is not obvious and that, for lift enhancement, they appear approximately equivalent. Compared to the open slot CFJ, the DCFJs only show improvement for OF higher than 1/2. While DCFJ 1/2 show only a 10% increase in lift, DCFJ 2/3 and DCFJ 3/4 show a 30% to 50% increase. These results are considerable considering the magnitude of lift achievable and the energy expenditure of the CFJ pump. For example, using the DCFJ 2/3 at $C_{\mu}^* = 0.08$ provides comparable lift coefficient with the open slot CFJ that needs twice the flow rate. As can be seen in Fig. 11, for open slot CFJ, the maximum lift is increased by 1.5 to 1.8 times. For DCFJ 3/4, the maximum lift is increased by 2.73 times using the same mass flow rate as the open slot CFJ airfoil.

Obstruction Factor(OF) Effect on Drag

Drag coefficient C_D for baseline, open slot and all DCFJ configurations are grouped together in Fig. 10. Similarly to the lift results, DCFJ 1/5 and DCFJ 1/3 show only a small decrease in drag compared to the open slot CFJ. Negative values of drag are observed with increased range of AoA. For OF larger than 1/2, a significant drag reduction is observed for all C_{μ}^* . A large difference between DCFJ 2/3 and DCFJ 3/4 is observed: while being comparable for lift increase, DCFJ 3/4 shows lower drag than DCFJ 2/3. Negative values of drag are observed for AoA up to 30° . The negative drag is created by the co-flow jet filling the wake and the supersuction effect at LE [17, 18, 19, 20]. DCFJs are seen to provide increased values of thrust, with up to 4 times of the thrust of the open slot CFJ airfoil. These results are significant since this negative drag / thrust component can effectively reduce the overall drag of an aircraft or helicopter rotor blade, providing a significant reduction in the engine power required to move the aircraft or rotate the rotor blades.

Combined Effect of Lift and Drag

The net lift increase and drag reduction for all configurations are plotted in Fig. 12. All DCFJ airfoils (with $OF > 1/2$) show net lift augmentation that intensifies with increasing values of C_{μ}^* and grows linearly with AoA. The drag reduction is nearly constant at different AoA for a fixed C_{μ}^* . Similar to the lift augmentation, the higher the value of C_{μ}^* is, the larger the drag is reduced. This drag reduction can be so large that thrust is generated (Fig. 10).

Fig. 13 shows the drag polar curves for all the configurations. Compared with the baseline airfoil without flow control, the CFJ airfoil drag polars shift to the left and upward due to the high thrust and high lift. The drag polar shape in Fig. 13 is unconventional. The CFJ airfoil generates a very large lift and thrust at the same time. In nature, only the birds' flapping wings have such an effect. The CFJ airfoils achieves the same effect, but using a fixed wing.

Fig. 14 shows the drag reduction efficiency for all the CFJ airfoils. The open slot CFJ results range from 40% to 70%, depending on the value of C_{μ}^* . Results for DCFJ with $OF=1/2$ are somewhat comparable with open slot CFJ. But for $OF>1/2$, the drag reduction efficiency is found to reach higher value, approaching ~80% for all AoA and all C_{μ} . This means that the energy cost to generate injection jet momentum not only benefits the system with a significant lift gain, but also transfers nearly 80% of jet momentum to drag reduction. Hence the overall energy expenditure is small compared to the efficiency gain measured as the ratio of lift to drag L/D .

Stall Angle Delay

In addition to the enhancement of lift and drag reduction, CFJ airfoils also significantly increase stall AoA for the thick airfoil tested in [19,20]. In this research, the stall margin is also remarkably increased for the tested thin airfoil, especially for high OF , as can be seen in Fig. 10. For DCFJ 2/3 and DCFJ 3/4, stall angle is approximately 30° , a 30% increase from the baseline airfoil stall angle of 23° . Higher stall AoA gives more stall margin and increases the safety of aircraft.

Power Consumption

The airfoil performance enhancement due to flow control must come at a cost of energy consumption. It is hence very important to evaluate the energy expenditure of a flow control method. To calculate the power consumption based on Eq. (3), a series of tests was made to measure the total pressure and temperature at the injection and suction cavity, respectively (see Fig. 3). The efficiency of the pumping system is not considered since it will vary with different pumping implementation. In this research, the pumping system efficiency, η_p was taken as 100%.

The measured total pressure ratio inside the injection and suction cavities and the corresponding power coefficient are shown in Fig. 15 through 17 for three AoA and three C_{μ}^* . The power consumption value is also placed on the same graph. The results for open slot CFJ are shown Fig. 15. A very low pressure difference (about 1.2kPa) is sufficient to maintain the open slot CFJ and therefore a low power is required. The maximum power required for the open slot CFJ airfoil is about 60W. The power coefficient is smaller than 1 for all AoA and all C_{μ}^* . The pressure ratio and power required are slightly reduced when the AoA is increased. The results for CFJ 2/3 are shown in Fig. 16. The pressure difference increases to about 12kPa, producing a pressure ratio increase of about 10%. In turn, the power consumption increases to 600W (a factor of 10 increase) for the maximum power required with power coefficient between 0.9 and 5.5. The higher power consumption of DCFJ than open slot CFJ is because the flow suffers more energy loss going through multiple smaller holes than going through one large slot. The AoA appears to have little effect on the pressure ratio and power consumption for DCFJ.

Finally, a comparison of the high-performance DCFJs with open slot CFJ is shown in Fig. 17. For each configuration, only the highest pressure and power for all AoA were retained. The pressure ratio increases substantially for increasing OF but never reach values beyond 1.2. The resulting power consumption also increases, but this increase is paid off with the higher lift and thrust gain. The DCFJ 2/3 power consumption is about 10 times higher than the open slot CFJ. In turn, the DCFJ 3/4 power consumption is only 10% higher than the DCFJ 2/3.

IV. Conclusion

The performance enhancement of the CFJ airfoil is demonstrated in this paper by using discrete jets over a single open slot jet. The hypothesis is that a DCFJ airfoil will generate both streamwise and spanwise vortex structures to achieve more effective turbulent mixing than an open slot CFJ airfoil. The configurations with higher number discrete jets and smaller jet sizes show significantly better performance enhancement for all flow rates. Compared to an open slot CFJ airfoil using the same mass flow rate, a discrete CFJ airfoil can provide an additional 50% increase in maximum lift, 30% stall AoA increase, and 300% drag reduction. The drag reduction is striking, and in most of the cases a very large thrust can be generated. The DCFJ airfoil with more injection jets and large obstruction factor, namely DCFJ 2/3 and DCF 3/4, provide the greatest performance enhancement. While the lift in both cases is comparable, the DCFJ 3/4 supplies an additional 10% increase in thrust compared to DCFJ 2/3. The pumping pressure ratio and power consumption are increased by reducing the injection jet size and increasing the number of jets. For all the tests shown here, the pumping pressure ratio remained under 1.2. The DCFJ power consumption is about 10 times higher than that for open slot CFJ, and is up to 600W. Nearly 80% of the injection momentum is translated to drag reduction, which indicates that a CFJ airfoil is highly energy efficient. These results demonstrate that the DCFJ airfoil outperforms the original open slot CFJ airfoil. An optimum choice of injection jet number and size is crucial to determine the maximum performance enhancement at lowest energy expenditure. More work need to be done in this area. Based on the results presented here, the DCFJ airfoil concept may play an important role in the development of future integrated airframes-propulsion systems and rotorcraft systems.

Acknowledgement

The support for this research under ARO/AFOSR Grant 50827-RT-1SP is acknowledged.

REFERENCES

- [1] W. L. I. Sellers, B. A. Singer, and L. D. Leavitt, "Aerodynamics for Revolutionary Air Vehicles." AIAA 2004-3785, June 2003.

- [2] M. Gad-el Hak, "Flow Control: The Future ," Journal of Aircraft, vol. 38, pp. 402–418, 2001.
- [3] M. Gad-el Hak, Flow Control, Passive, Active, and Reactive Flow Management. Cambridge University Press, 2000.
- [4] S. Anders, W. L. Sellers, and A. Washburn, "Active Flow Control Activities at NASA Langley." AIAA 2004-2623, June 2004.
- [5] C. P. Tilmann, R. L. Kimmel, G. Addington, and J. H. Myatt, "Flow Control Research and Application at the AFRL's Air Vehicles Directorate." AIAA 2004-2622, June 2004.
- [6] D. Miller, , and G. Addington, "Aerodynamic Flowfield Control Technologies for Highly Integrated Airframe Propulsion Flowpaths." AIAA 2004-2625, June 2004.
- [7] V. Kibens and W. W. Bower, "An Overview of Active Flow Control Applications at The Boeing Company." AIAA 2004-2624, June 2004.
- [8] R. Holman, Y. Utturkar, R. Mittal, and L. Cattafesta, "Formation Criterion for Synthetic Jets," AIAA Journal, vol. 43, No. 10, pp. 2110–2116, 2005.
- [9] T. C. Corke and M. L. Post, " Overview of Plasma Flow Control: Concepts, Optimization, and Applications." AIAA Paper 2005-0563, Jan. 2005.
- [10] C. Enloe, T. E. McLaughlin, G. I. Font, and J. W. Baughn, " Frequency Effects on the Efficiency of Aerodynamic Plasma Actuator ." AIAA Paper 2006-0166, Jan. 2006.
- [11] Raman, G. , " Using controlled unsteady fluid mass addition to enhance jet mixing. ," AIAA Journal, vol. 35, No. 4, pp. 647–656, 1997.
- [12] Freund, J.B. and Moin, P. , " Jet mixing enhancement by high-amplitude fluidic actuation," AIAA Journal, vol. 38, No. 10, pp. 1863–1870, 2000.
- [13] N. Wood and J. Nielsen, "Circulation Control Airfoils-Past, Present, Future." AIAA Paper 85-0204, 1985.
- [14] R. J. Englar, "Circulation Control Pneumatic Aerodynamics: Blown Force and Moment Augmentation and Modifications; Past, Present and Future." AIAA 2000-2541, June 2000.
- [15] M. Wilson and C. von Kerczek, "An Inventory of Some Force Procedure for Use in Marine Vehicle Control." DTNSRDC-791097, Nov, 1979.

- [16] G. S. Jones, "Pneumatic Flap Performance for a 2D Circulation Control Airfoil, Steady & Pulsed." Applications of Circulation Control Technologies, Chapter 7, p. 191-244, Vol. 214, Progress in Astronautics and Aeronautics, AIAA Book Series, Editors: Joslin, R. D. and Jones, G. S., 2006.
- [17] G.-C. Zha, W. Gao, and C. Paxton, "Jet Effects on Co-Flow Jet Airfoil Performance," AIAAJournal, No. 6,, vol. 45, pp. 1222–1231, 2007.
- [18] G.-C. Zha and D. C. Paxton, "A Novel Flow Control Method for Airfoil Performance Enhancement Using Co-Flow Jet." Applications of Circulation Control Technologies, Chapter 10, p. 293-314, Vol. 214, Progress in Astronautics and Aeronautics, AIAA Book Series, Editors: Joslin, R. D. and Jones, G.S., 2006.
- [19] G.-C. Zha, C. Paxton, A. Conley, A. Wells, and B. Carroll, "Effect of Injection Slot Size on High Performance Co-Flow Jet Airfoil," AIAA Journal of Aircraft, vol. 43, 2006.
- [20] G.-C. Zha, B. Carroll, C. Paxton, A. Conley, and A. Wells, "High Performance Airfoil with Co-Flow Jet Flow Control," AIAA Journal, vol. 45, 2007.
- [21] B.-Y. Wang, B. Haddoukessouni, J. Levy and Zha, G.-C., "Numerical Investigations of Injection Slot Size Effect on the Performance of Co-Flow Jet Airfoil", AIAA Journal of Aircraft, Vol. 45, No. 6, 2008, pp.2084-2091
- [22] B.-Y. Wang and G. Zha, "Detached-Eddy Simulation of a Co-Flow Jet Airfoil at High Angle of Attack", AIAA Paper 2009-4015, 39th AIAA Fluid Dynamics Conference, 22-25 June 2009, San Antonio, TX
- [23] B.P.E. Dano, D. Kirk, and G. Zha, "Experimental Investigation of Jet Mixing Mechanism of Co-Flow Jet Airfoil", AIAA-2010-4421, 5th AIAA Flow Control Conference, 28 Jun - 1 Jul 2010, Chicago, IL
- [24] G.-C. Zha, J. Dussling, S. Aspe, N. Heinz, and D. Martinez, "Quiet Ultra- Efficient Integrated Aircraft Using Co- Flow Jet Flow Control ", AIAA Paper 2009-1437, 47th AIAA Aerospace Sciences Meeting, 5 - 8 Jan. 2009, Orlando, FL
- [25] P. X. Coronado, B. Cuffie, D. Saer and G.-C. Zha, "Conceptual Design of a Personal Aerial Vehicle Using Co-Flow Jet Airfoil", AIAA Paper 2007-4442 25th AIAA Applied Aerodynamics Conference, June 25-28, 2007
- [26] J. Aguirre, B. Wang and G. Zha, "Conceptual Design and Study of ``Engineless" Airplane Using Co-Flow Jet Airfoil", AIAA Paper 2007-4441 25th AIAA Applied Aerodynamics Conference, June 25-28, 2007

[27] J. Aguirre, V. Casado, N. Chamie, and G. Zha, "Mars Intelligent Reconnaissance Aerial and Ground Explorer (MIRAGE)", AIAA Paper 2007-0244 AIAA 45th Aerospace Sciences Meeting and Exhibit, Reno, NV, Jan. 8-11, 2007

[28] Brown G.L., and Roshko A., "On density effects and large structure in turbulent mixing layers", J. Fluid Mech., Vol. 64, 1974, pp. 775-816.

[29] B.P.E Dano, and J.A. Liburdy, "Vortical Structure of a 45° Inclined Pulsed Jet in a Crossflow", AIAA-2006-3543, 2006.

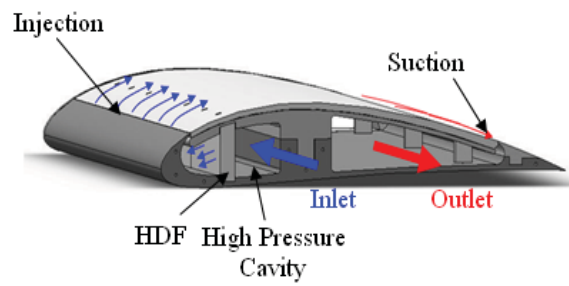


Fig.1. Schematic and concept of CFJ airfoil

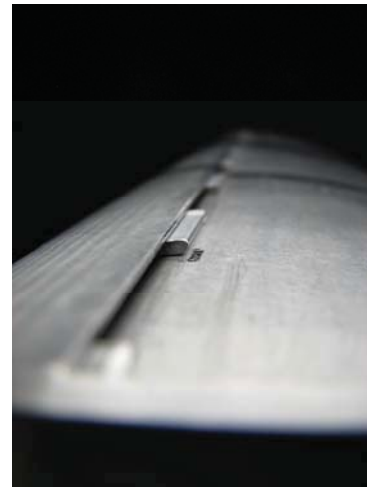


Fig. 2 Close up picture of the injection holes and tabs in position (Case 2B)

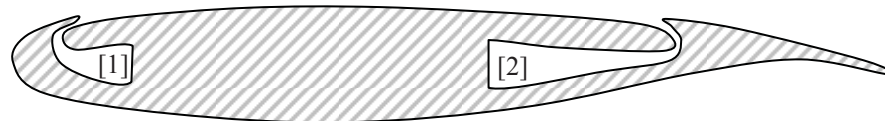


Fig.3. Probe location for total pressure and power measurement

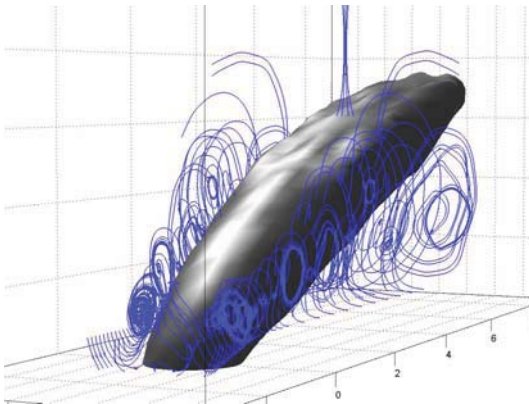


Fig. 4 Flow structure of a single 45° inclined jet, obtained from stereo-PIV. In dark-grey is the V_{jet} isosurface of velocity, and blue are 2D streamlines in the spanwise direction.

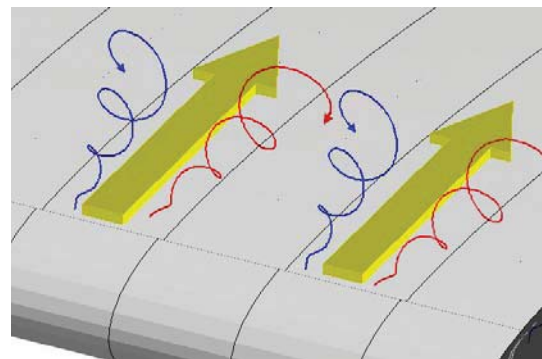


Fig. 5 Schematic of Counter Rotating Vortex Pairs (CVP) issued from a row of co-flow jets

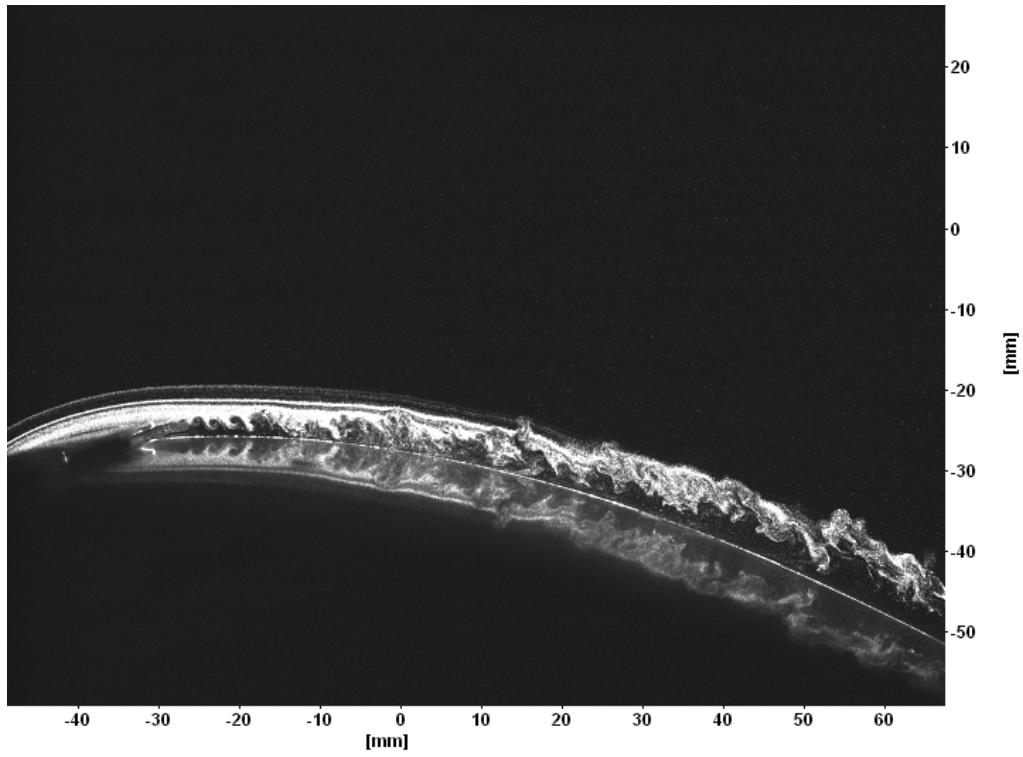


Fig. 6 Flow visualization along a discrete jet: DCFJ 3/4, $AoA=15^\circ$ and $C_\mu=0.08$.

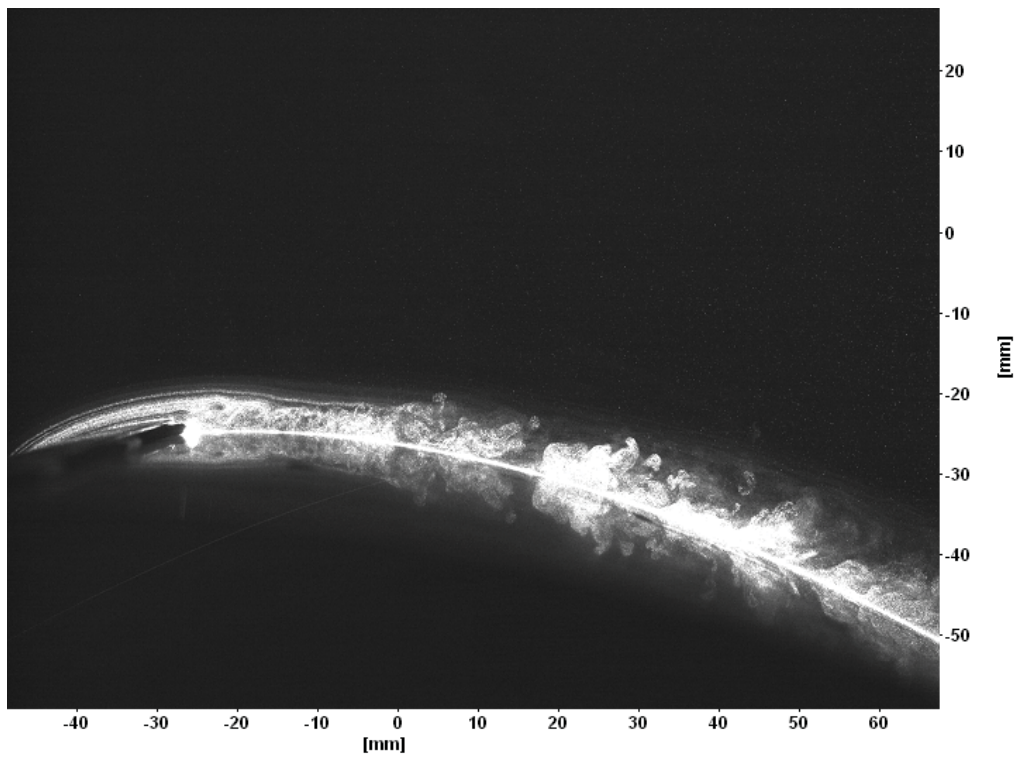


Fig. 7 Flow visualization over a tab: DCFJ 3/4, $AoA=15^\circ$ and $C_\mu=0.08$.

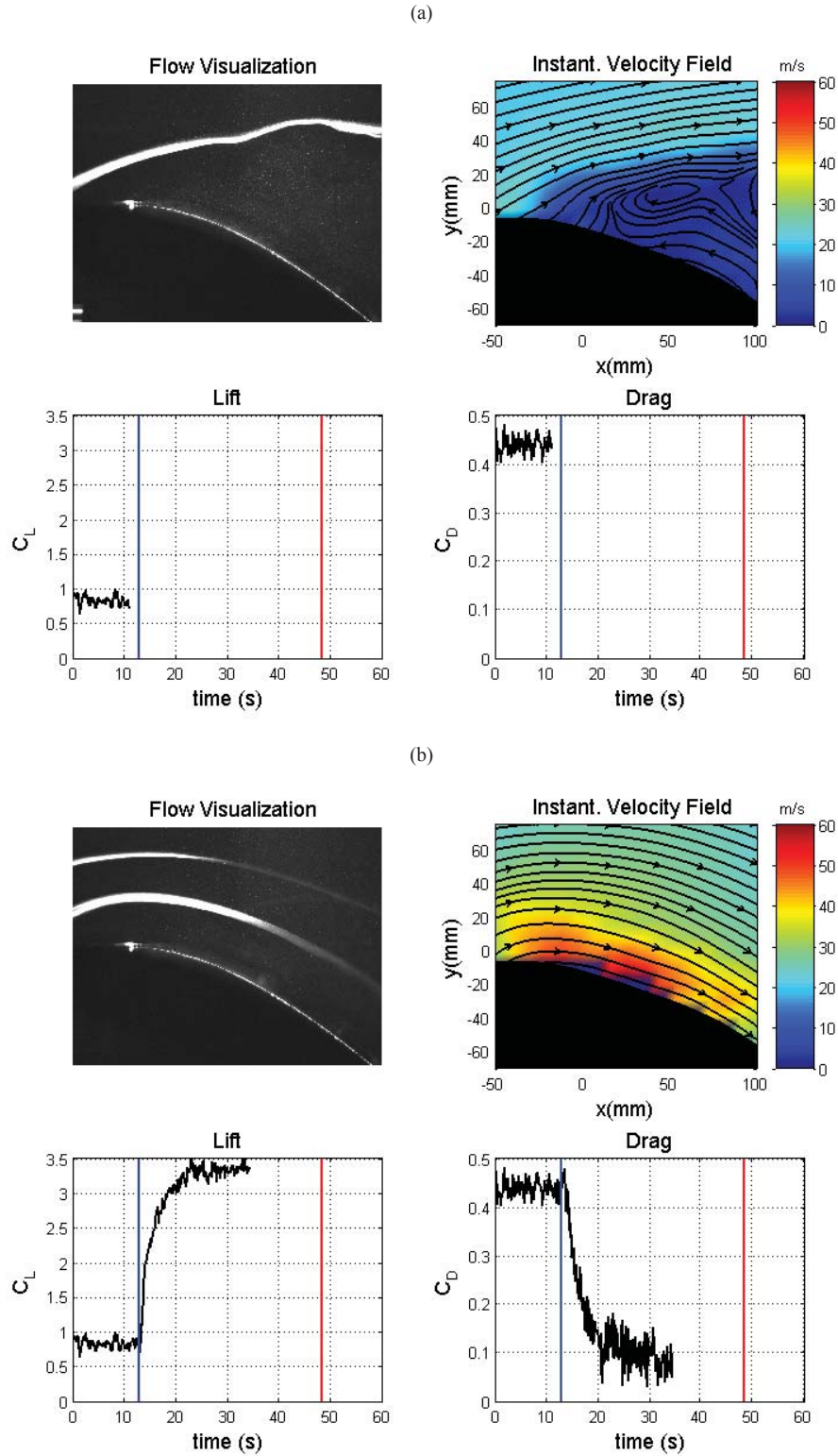


Fig. 8 Snapshots from video montage of simultaneous flow visualization, PIV velocity field, C_L and C_D at two instant in time during CFJ activation for DCFJ 2/3 with $C_{\mu}^* = 0.16$ and $AoA = 25^\circ$.

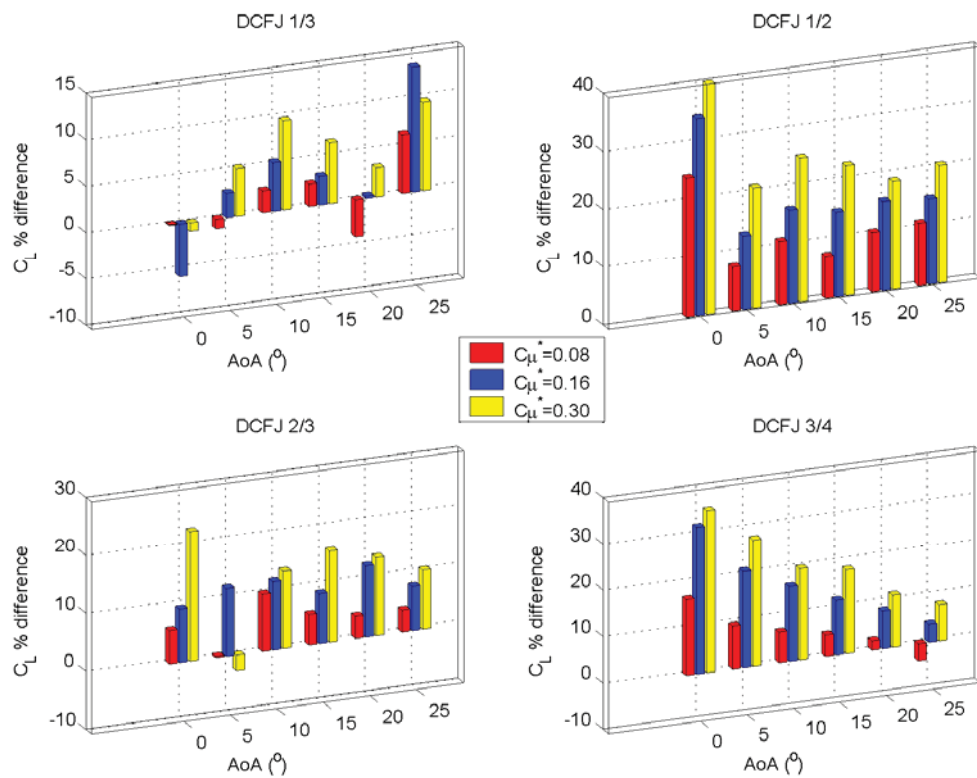


Fig. 9 Lift difference between DCFJ configuration A and configuration B

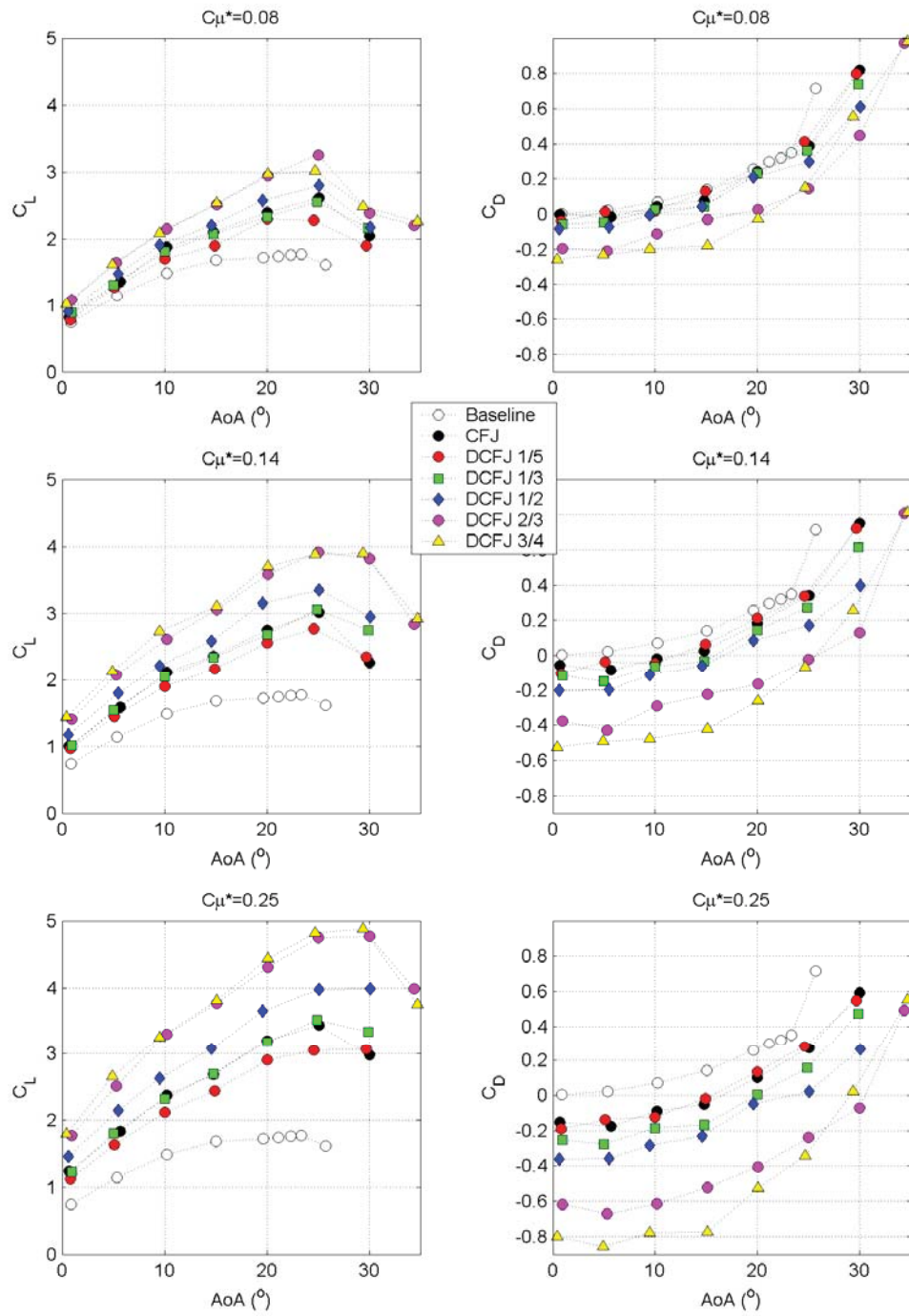


Fig. 10 Lift and Drag coefficients for all CFJ and DCFJ configurations

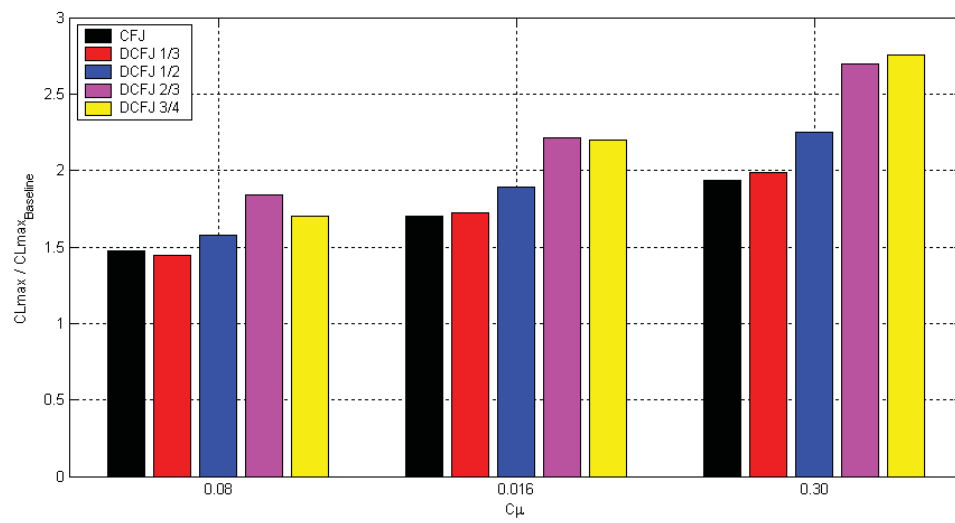


Fig. 11 Ratio of $CL_{\max}(CFJ) / CL_{\max}(\text{baseline})$ for all configurations and all C_μ^*

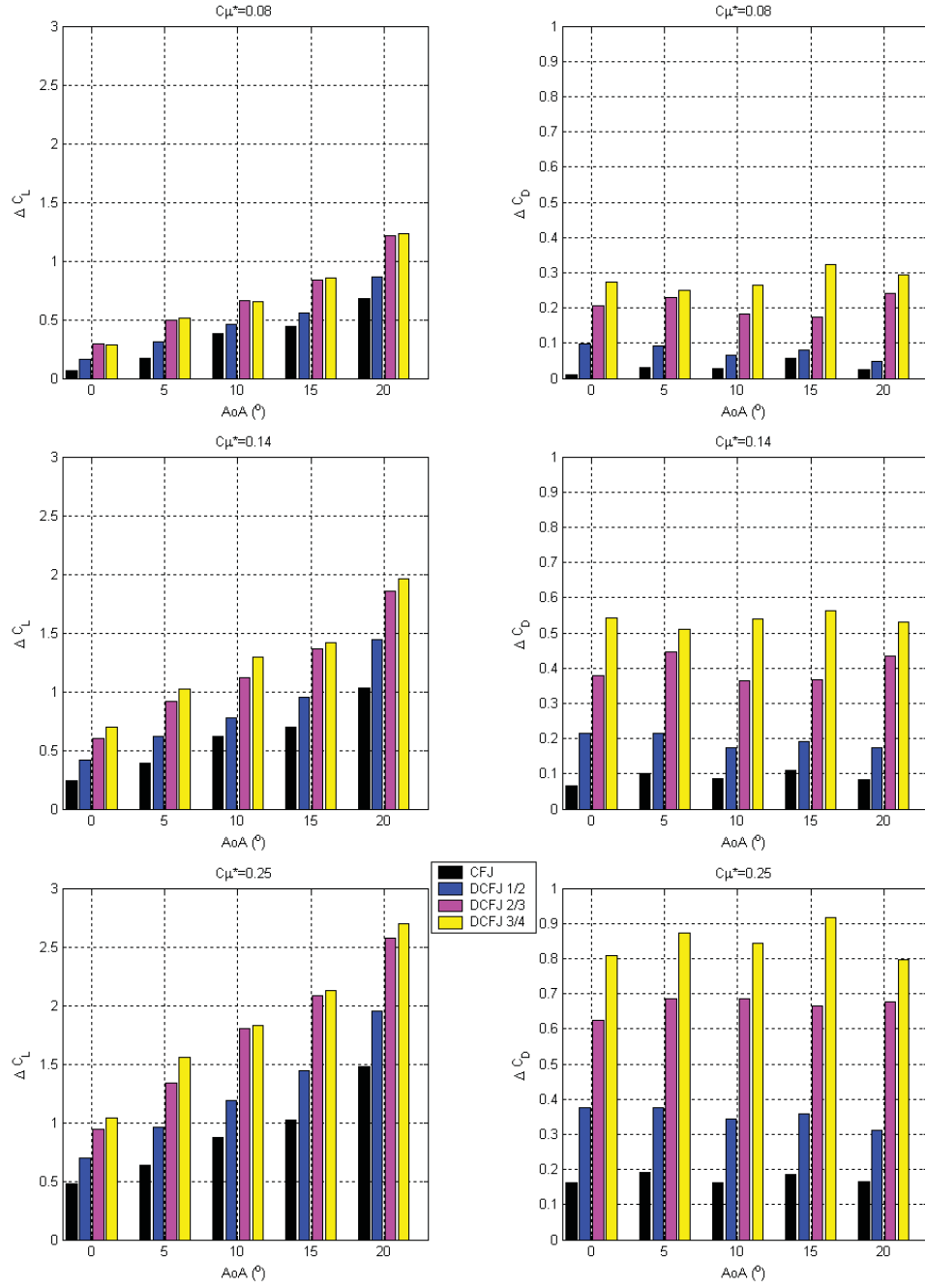


Fig. 12 Lift increase and drag reduction from Baseline, for CFJ and DCFJs at various C_{μ}^*

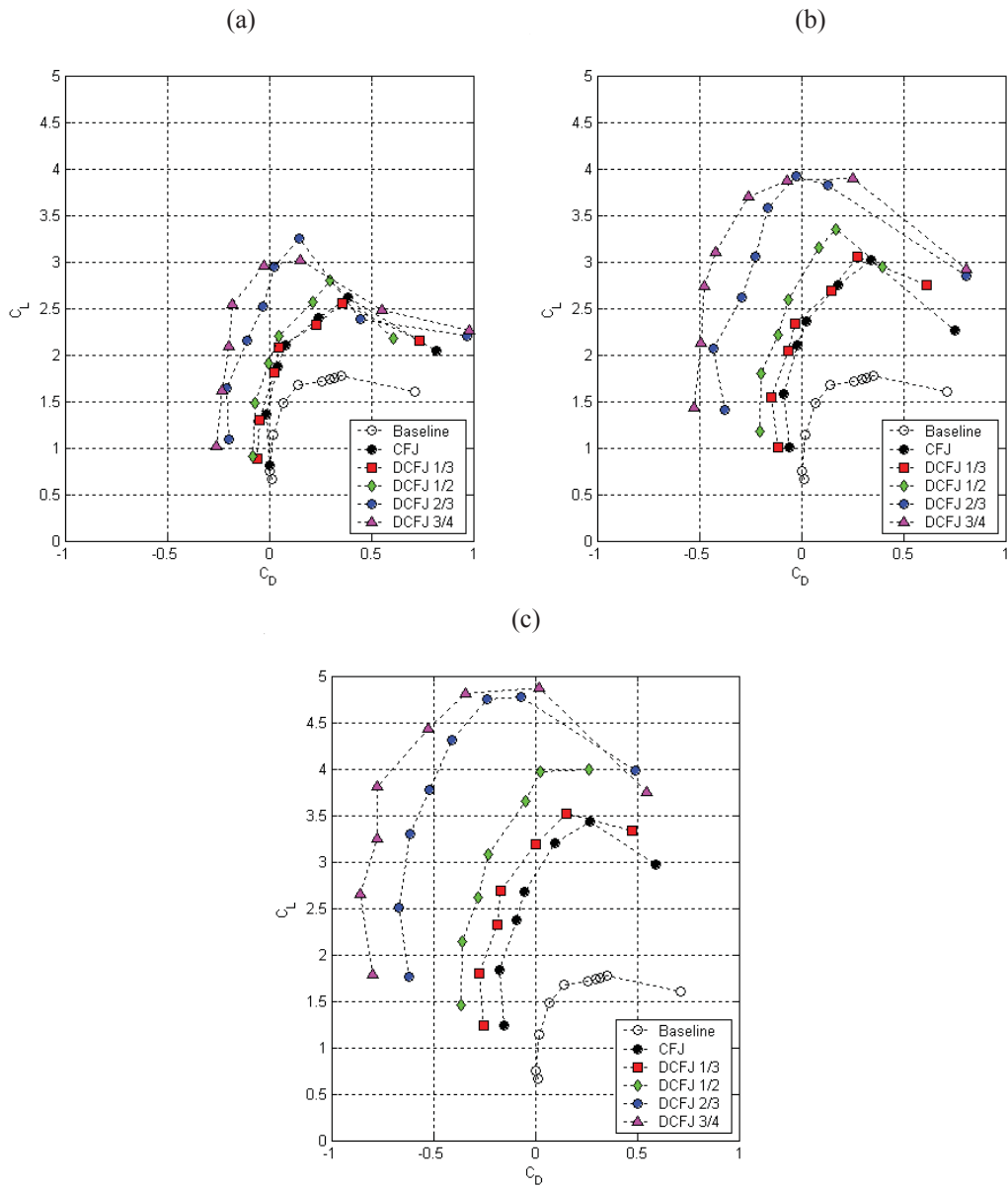


Fig. 13 Drag polars for all configurations (a) $C_\mu^* = 0.08$, (b) $C_\mu^* = 0.14$ and (c) $C_\mu^* = 0.25$

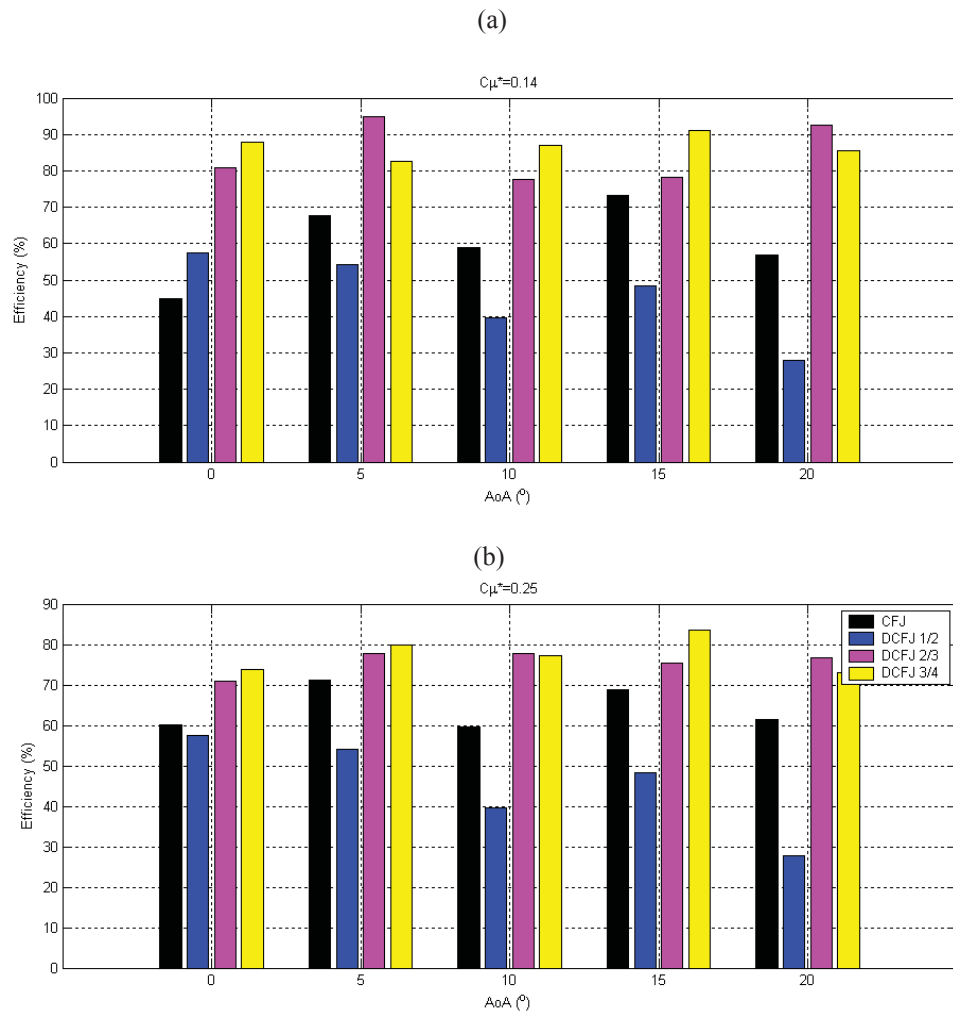


Fig. 14. Drag reduction efficiency vs AoA for (a) $C_{\mu}^* = 0.08$ (b) $C_{\mu}^* = 0.25$

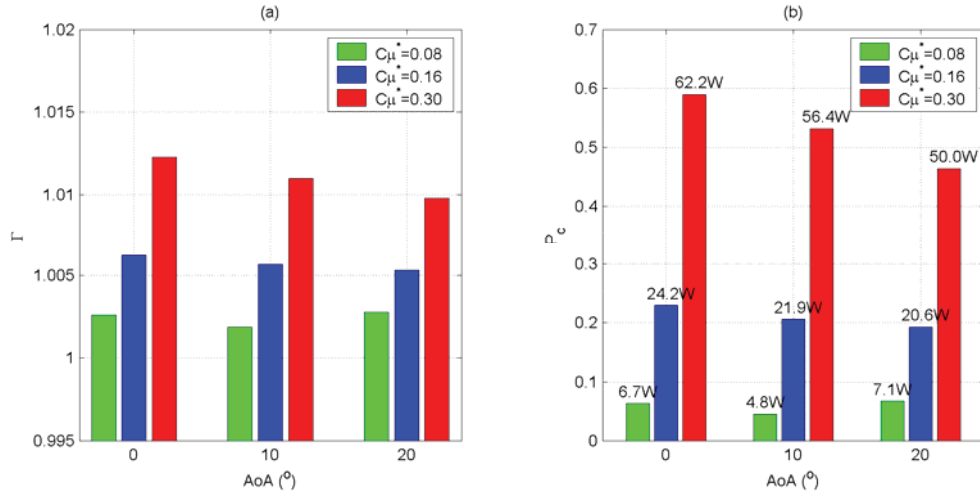


Fig. 15 Power consumption results for the open slot CFJ. (a) Pressure ratio (b) Power coefficient

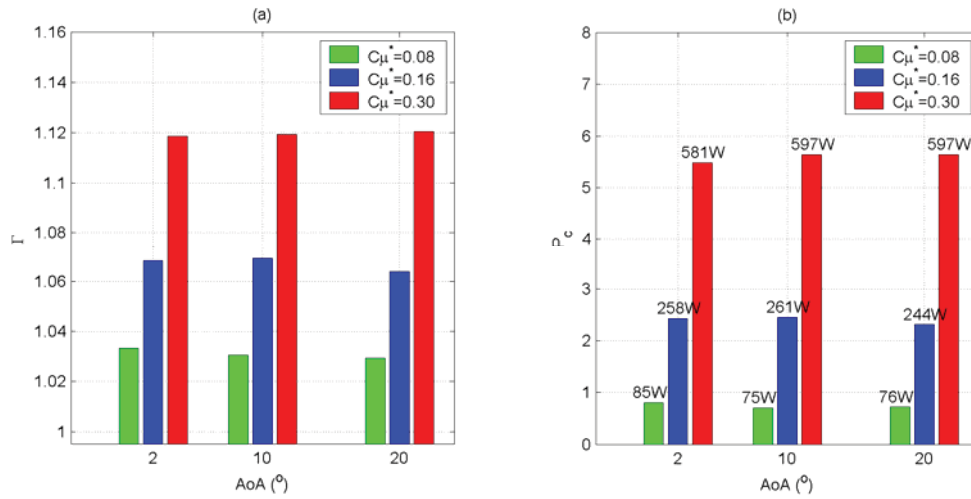


Fig. 16 Power results for the DCFJ 2/3. (a) Pressure ratio (b) Power coefficient

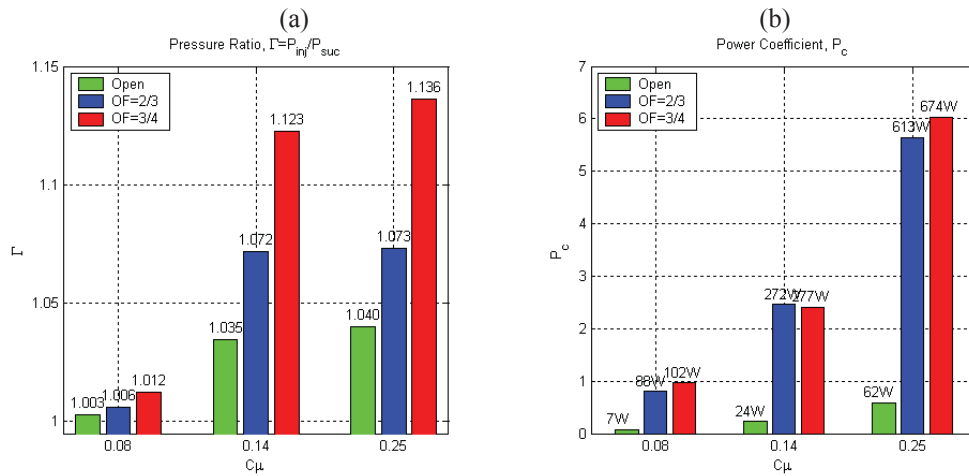


Fig. 17 Power results for the open slot CFJ. (a) Pressure ratio (b) Power coefficient